Experimental and Computational Studies of Four-Coordinate Aluminum: The Reaction of Aluminates and Acids

Robert Damrauer,*,† Michèle Krempp,† Niels H. Damrauer,† Michael W. Schmidt,‡,§ and Mark S. Gordon*,‡,§

Contribution from the Department of Chemistry, University of Colorado at Denver, Denver, Colorado 80217-3364, and Chemistry Department, North Dakota State University, Fargo, North Dakota 58105-5516

Received May 29, 1992. Revised Manuscript Received November 19, 1992

Abstract: The gas-phase reactions of trimethylaluminates with a variety of acids are considered from both an experimental and computational perspective. The experimental work involves product and kinetic studies of ten aluminates, $[(CH_3)_3AlX]^-$ (X = H, CH_3, NH_2, OH, F, SiH_3, PH_2, SH, Cl, and OCH_3). Both X and methyl cleavage pathways are observed in these reactions. X cleavage occurs with several aluminates (X = H, NH_2, OH, and PH_2), in contrast to the thermochemical predictions of *ab initio* computations performed at the MP2/6-31++G(d,p) level. These indicate that methyl cleavage is favored in the reaction of nine aluminates (OCH_3 was not computed) and HCl. Kinetic studies show a wide range of reactivities for these aluminates. *Ab initio* calculations also give estimates of the X^- affinities for $(CH_3)_3Al$ and the Cl^- and CH_3^- affinities of $(CH_3)_2AlX$. Analogous semiempirical computations of these aluminates using MNDO, AM1, and PM3 techniques give unreliable results compared to the *ab initio* computations and have no utility even for qualitative estimates. Computational studies of the reaction paths for $[(CH_3)_3AlX]^-$ (for X = F and OH) with HCl as well as intrinsic reaction coordinate calculations for $[(CH_3)_3AlF]^-$ + HCl leading from the transition state to products have also been carried out. These computations not only describe the transition states, but properly predict the cleavage results for X and methyl cleavage. The intrinsic reaction coordinate calculations give a qualitative interpretation of the reaction dynamics of $[(CH_3)_3AlF]^-$ plus HCl.

Introduction

One of the most important characteristics of an atom or molecule is its affinity for various species. Proton affinity, for example, is a measure of how susceptible a molecule is to protonation.[1] Neutral molecule, hydride, and halide affinities often provide information about the bonding characteristics of a metal atom in organometallic compounds.[1] Affinities are often determined in the gas phase where the obscuring effects of solvents and counterions can be eliminated.[1] Direct measurements, however, are rarely carried out; instead, either equilibrium or bracketing methods are used to determine gas-phase affinities.[2]

The studies reported in this paper were originally conceived to determine the affinity of monomeric trimethylaluminum for a number of anions using bracketing techniques similar to those applied by Squires and co-workers[2] in estimating the hydride affinities of silanes ($R_3R'Si$). By reacting reference acids (HA) of varying strength with siliconates (pentacoordinate silicon anions) in eq 1, these workers observed that the siliconates react

$$[R_3R'SiH]^- + HA \rightarrow R_3R'Si + H_2 + A^- \qquad (1)$$

with certain reference acids but not with other less acidic ones. Using these brackets as a determination[2] of the ΔH_{rxn} and combining them with the known gas-phase acidities of HA and H_2 allowed an estimate of the H^- affinity of the corresponding silanes (line A, Scheme I).[2] The results of Squires and co-workers were consistent with several *ab initio* computational studies reporting silane hydride affinities.[2,3]

Scheme I

(A) $[R_3R'SiH]^-$	$\rightarrow R_3R'Si + H^-$	$\Delta H^\circ_{H^-\text{Affinity of } R_3R'Si}$
(B) HA	$\rightarrow H^+ + A^-$	$\Delta H^\circ_{acid(HA)}$
(C) $H^+ + H^-$	$\rightarrow H_2$	$-\Delta H^\circ_{acid(H_2)}$

$$[R_3R'SiH]^- + HA \rightarrow R_3R'Si + H_2 + A^- \quad (1)$$

$$\Delta H_{rxn} = \Delta H^\circ_{H^-\text{Affinity of } R_3R'Si} + \Delta H^\circ_{acid(HA)} - \Delta H^\circ_{acid(H_2)}$$

In this paper we report on some of the experimental aspects of our attempts to measure the X^- affinity of trimethylaluminum using an analogous bracketing technique. We have prepared ten aluminates, $[(CH_3)_3AlX]^-$, and studied their reaction chemistry with reference acids using flowing afterglow-selected ion flow tube technology. Although a narrow bracketing range can be found for each aluminate (X = H, CH_3, NH_2, OH, F, SiH_3, PH_2, SH, Cl, and OCH_3) reacting with the reference acids, a simple interpretation based on Squires' siliconate precedent fails since more than one reaction pathway has been observed for the aluminates. A thorough understanding of the reaction chemistry of aluminates with acids thus involves a more complete study. We report on the major aspects of these reactions in this paper combining experimental and computational approaches.

Experimental Section

All experiments are carried out at room temperature in a tandem flowing afterglow-selected ion flow tube (FA-SIFT) described in detail previously.[4] Briefly, the FA-SIFT consists of four sections: a source (first) flow tube for ion preparation, an ion selection region, a second flow tube for studying the chemical reactions of the selected ions, and an ion

* Authors to whom questions should be addressed.
† University of Colorado at Denver.
‡ North Dakota State University.
§ Present address: Chemistry Department, Iowa State University, Ames, Iowa 50011.

(1) Bartmess, J. E. *Mass Spectrom. Rev.* **1989**, *8*, 297-343.
(2) Hajdasz, D. J.; Squires, R. R. *J. Am. Chem. Soc.* **1986**, *108*, 3139-3140.
(3) Damrauer, R.; Burggraf, L. W.; Davis, L. P.; Gordon, M. S. *J. Am. Chem. Soc.* **1988**, *110*, 6601-6.
(4) Van Doren, J. M.; Barlow, S. E.; Depuy, C. H.; Bierbaum, V. M. *Int. J. Mass Spectrom. Ion Processes* **1987**, *81*, 85-100.

0002-7863/93/1515-5218$04.00/0

detection region. In the typical experiment whose results are reported in this paper, aluminates are prepared in the first flow tube by reaction of trimethylaluminum dimer and X^-. The X^- ions are prepared in the source by electron impact on the appropriate neutral (e.g. NH_3 for H_2N^-). Both $[(CH_3)_3AlX]^-$, where X = CH_3 and H, had to be prepared by different means. Reaction of a higher concentration of trimethylaluminum dimer with H_2N^- gave the X = CH_3 aluminate and $[(CH_3)_3AlNH_2]^-$ in roughly equal amounts. The X = H aluminate was prepared from trimethylaluminum dimer and methoxide, presumably through the intermediacy of $[(CH_3)_3AlOCH_3]^-$. This methoxyaluminate has been shown to undergo CID to the X = H aluminate. A similar process may be occurring in the first flow tube. More than one product forms in the reactions leading to the X = CH_3 and H aluminates; however, the desired anions are readily mass selected as described below.

The aluminates are then entrained in a rapidly flowing helium stream (0.3 Torr) and, at the end of the first flow tube, are sampled through a nose cone orifice into the ion separation region. The helium and other neutrals are removed by pumping while the aluminates are focused into a quadrupole mass filter by a series of electrostatic lenses. This SIFT quadrupole can be tuned to an appropriate m/z and the desired aluminates are injected into the second flow tube, where they are entrained in helium (0.5 Torr).

The reactions of the injected aluminates can then be studied by the addition of a variety of acids in the second flow tube. At the end of the second flow tube, the ionic products are sampled through a nose cone orifice, mass analyzed, and detected by an electron multiplier. It is important to recognize that structures for the product ions discussed in this paper are based on a recording of their m/z and by chemical intuition. Neutral products are not detected, but they are assumed based on mechanistic rationale.

The product identification experiments are performed by reaction of the selected aluminates with reference acids (HA).[5] A typical aluminate reacts with a series of reference acids to give several characteristic products that will be discussed in the Results and Discussion section. The ion product recoveries in these reactions are virtually quantitative. For each of the aluminates, a bracket can be established between two reference acids, one which gives A^- and another which does not. In general, however, the reactions of aluminates and acids (HA) show anionic products of greater complexity, namely $[(CH_3)_3AlA]^-$ and $[(CH_3)_2AlX(A)]^-$. Such products indicate that both HX and methane cleavage channels are active. These will also be discussed in the Results and Discussion section.

Branching ratios for the reaction of the aluminates and acids were determined by injecting the aluminates into the second flow tube and adding a particular acid at various points along the second tube. These ratios were determined as a function of reaction distance and are reported as extrapolations to zero reaction distance to eliminate any effects of secondary reactions or differential diffusion among the ions. Mass discrimination corrections were made for all the reactions of HCl where branching ratios are reported except for $[(CH_3)_3AlH]^-$ where signal stability problems prevented it. Other branching ratios reported herein were carried out in an analogous manner. The reported branching ratios are reproducible to ±10%.

Rate coefficients were determined under pseudo-first-order conditions by monitoring the aluminate ion density as a function of reaction distance (which is proportional to time) with use of a measured flow of neutral acid reagent. Reported values are the average of at least three measurements with different flows and are reproducible to ±10%. Reaction efficiencies have been calculated from ion-neutral collision rates using the variational transition state theory model of Bowers and coworkers.[6]

To inject ions from the low-pressure (10^{-6} Torr) region of the SIFT quadrupole into the higher-pressure region of the second flow tube, they must be extracted by an electrical potential which imparts kinetic energy to them. Multiple collisions with the helium buffer gas generally cool such ions; however, if the potential is made sufficiently high, ions can often undergo collision-induced dissociation (CID) forming new ions.[7-11] In a field-free region, the resulting ions can subsequently undergo multiple collisions with helium where they are usually cooled to room temperature. The injection potential leading to decomposition of ions is the potential difference between the ion source and the injector plate. The resulting kinetic energy of the ions is a sensitive function of a variety of factors and is not well-characterized.

All reactions were studied at a He flow of ~225 STP cm^3 s^{-1}. Gases were obtained from commercial sources and were of the following purities: He (99.995%), NH_3 (99.99%), CH_4 (99.99%), and N_2O (99.99%). Other reagents were obtained from commercial sources. The helium buffer gas was passed through a liquid nitrogen cooled molecular sieve trap before entering the flow tubes.

Computational Details. All *ab initio* calculations were carried out with the GAMESS program.[12] Minima were located via closed shell SCF using the 6-31G(d) basis[13-16] for large molecules [this level can be summarized as RHF/6-31G(d)] and at the RHF/6-31++G(d,p) level[17] for small isolated X^- ions. We have previously found[18-20] that geometry optimizations on large, closed shell anions do not have large errors when diffuse functions are omitted from the basis. This approach was explicitly tested in this work by optimizing $[(CH_3)_4Al]^-$ with the 6-31G(d) basis and then reoptimizing with the 6-31++G(d,p) basis. The second optimization changes the Al–C bond length from 2.0501 t0 2.0495 Å and lowers the energy by just 0.1 kcal/mol. Thus, large, closed shell anions do not require diffuse functions for their geometry optimization. In contrast, closed shell X^- systems containing only a single heavy atom do not have a large spatial extent over which to spread the extra charge. These show somewhat larger changes when diffuse functions are included in the geometry optimization. The largest change we found for geometry optimization of X^- with diffuse functions occurred for CH_3^-, where the bond length shortens by 0.023 Å and the energy decreases by 1.9 kcal/mol relative to the 6-31G(d) structure. Because the X^- anions are small, it is straightforward to find their structures at this somewhat improved level, so this was done. The *ab initio* optimized structures were verified to be minima on the respective potential energy surfaces by calculating matrices of energy second derivatives (hessians). In each case the hessian is positive definite as required for a minimum energy structure.

Although structure predictions of large, closed shell anions do not require diffuse functions, the inclusion of these functions is critical for accurate energy results. We have performed single point energy calculations at both the RHF and MP2[21-23] levels using the 6-31++G(d,p) basis. Dramatic changes in the RHF energetics occur upon addition of the diffuse functions. For example, the electronic energy change for $(CH_3)_3Al + H^- \rightarrow [(CH_3)_3AlH]^-$ is −100.1, −64.6, and −71.3 kcal/mol at the RHF/6-31G(d), RHF/6-31++G(d,p), and MP2/6-31++G(d,p) levels. The diffuse functions typically cause a 5–40 kcal/mol change in the RHF energies. Inclusion of electron correlation at the MP2 level changes the energetics by 1–15 kcal/mol with the majority of the reactions we considered changing by 5–10 kcal/mol.

Since there are large changes in the RHF energetics upon basis improvement, we have performed an RHF calculation in an extended basis for every reaction considered in the present work. This basis was the identical DZP quality basis for hydrogen atoms, but it used an approximately triple-ζ (6-311G or McLean/Chandler) basis,[24-26] aug-

(5) All of the thermochemical values cited in this paper are from the following: Lias, S. G.; Bartmess, J. E.; Liebman, J. F.; Holmes, J. L.; Levin, R. D.; Mallard, W. G. In *J. Phys. Chem. Ref. Data, Suppl. No. 1* **1988**, *17*.

(6) Chesnavich, W. J.; Su, T.; Bowers, M. T. *J. Chem. Phys.* **1980**, *72*, 2641–55.

(7) Gronert, S.; O'Hair, R. A. J.; Prodnuk, S.; Sülzle, D.; Damrauer, R.; DePuy, C. H. *J. Am. Chem. Soc.* **1990**, *112*, 997–1003.

(8) Damrauer, R.; Krempp, M. *Organometallics* **1990**, *9*, 999–1004.

(9) Damrauer, R.; Krempp, M. *Organometallics* **1990**, *9*, 1353–5.

(10) Damrauer, R.; Krempp, M.; Schmidt, M. W.; Gordon, M. S. *J. Am. Chem. Soc.* **1991**, *113*, 2393–2400.

(11) Damrauer, R.; Krempp, M.; O'Hair, R. A. J. *J. Am. Chem. Soc.* **1993**, *115*, 1998–2005.

(12) Schmidt, M. W.; Baldridge, K. K.; Boatz, J. A.; Jensen, J.; Koseki, S.; Gordon, M. S.; Nguyen, K. A.; Windus, T. L.; Elbert, S. T. *QCPE Bull.* **1990**, *10*, 52–54. For additional information on this program, contact MWS at mike@si.fi.ameslab.gov.

(13) Hehre, W. J.; Ditchfield, R.; Pople, J. A. *J. Chem. Phys.* **1972**, *56*, 2257–2261.

(14) Francl, M. M.; Pietro, W. J.; Hehre, W. J.; Binkley, J. S.; Gordon, M. S.; DeFree, D. J.; Pople, J. A. *J. Chem. Phys.* **1982**, *77*, 3654–3665.

(15) Gordon, M. S. *Chem. Phys. Lett.* **1980**, *76*, 163–168.

(16) Hariharan, P. C.; Pople, J. A. *Theor. Chim. Acta* **1973**, *28*, 213–222.

(17) (a) d exponent for H is 1.0 from ref 20. (b) p exponents for Al, P, S, and Cl are 0.325, 0.55, 0.65, and 0.75 from ref 18. (c) p exponent for Si is 0.395 from ref 19. (d) Diffuse s exponent for H is 0.036, diffuse sp exponents are C (0.034), N (0.048), O (0.059), F (0.074), Si (0.027), Al (0.017), P (0.035), and Cl (0.049) taken from the following: Clark, T.; Chandrasekhar, J.; Spitznagel, G. W.; Schleyer, P. von R. *J. Comput. Chem.* **1983**, *4*, 294–301.

(18) Gordon, M. S.; Davis, L. P.; Burggraf, L. W.; Damrauer, R. *J. Am. Chem. Soc.* **1986**, *108*, 7889–93.

(19) Davis, L. P.; Burggraf, L. W.; Gordon, M. S. *J. Am. Chem. Soc.* **1988**, *110*, 3056–62.

(20) Gordon, M. S.; Davis, L. P.; Burggraf, L. W. *J. Phys. Chem.* **1990**, *94*, 8125–8128.

(21) Carsky, P.; Hess, B. A.; Schaad, L. J. *J. Comput. Chem.* **1984**, *5*, 280.

(22) Møller, C.; Plesset, M. S. *Phys. Rev.* **1934**, *46*, 618.

(23) Pople, J. A.; Binkley, J. S.; Seeger, R. *J. Quantum Chem. Symp.* **1976**, *S10*, 1–19.

Scheme II

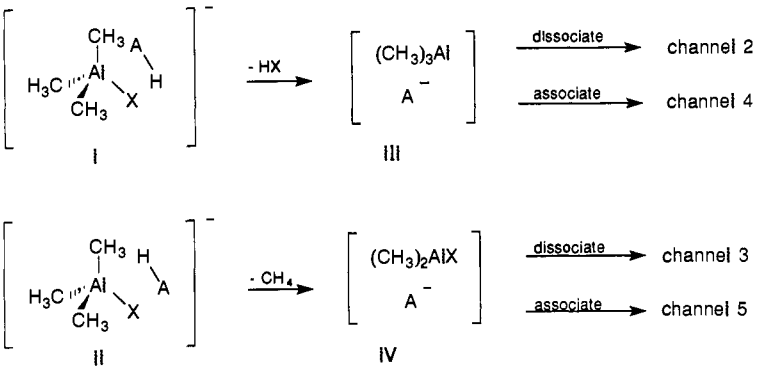

mented by diffuse functions and two sets of d polarization functions on all heavy atoms. These RHF/TZ++(2d,p) calculations show that the RHF/6-31++G(d,p) calculations are pretty well converged for the present systems. For example, the extended basis RHF energy for the reaction cited in the preceding paragraph is -64.8 kcal/mol. The changes in RHF energetics are typically 1-2 kcal/mol and thus are considerably smaller than the MP2 corrections mentioned above. In view of the small effect of basis improvements at the RHF level, we have not attempted to include these 1-2 kcal/mol corrections.

All energy results presented in this paper are therefore derived from MP2/6-31++G(d,p) calculations with appropriate thermochemical corrections applied. Zero-point energies and other necessary thermochemical data are taken from the same basis as used for structural determinations. Standard statistical mechanical approximations (ideal gas, rigid rotor, harmonic oscillator) are used to convert the electronic energies, unscaled frequencies, and moments of inertia to ΔH and ΔG at T = 298 K.

The *ab initio* computations on the transition states were carried out using the same methods as those just described. The transition states were located at the RHF/6-31G(d) level and characterized as such by computation of the energy hessian. Energetic results reported here are derived from MP2/6-31++G(d,p) calculations corrected to ΔH(298K) or ΔG(298K) by statistical mechanics. RHF calculations with the extended TZ++(2d,p) basis were performed, and were found to raise all four barriers reported below by about 1-2 kcal/mol. Since the 6-31++G(d,p) basis again seems well-converged, only MP2 results with this basis are presented here.

MNDO, AM1, and PM3 semiempirical computations were carried out using the MOPAC program with full geometry optimization (using the PRECISE option).[27] Since the semiempirical methods give an inadequate treatment of isolated small anions,[3,19] we used experimental heats of formation[5] for all the isolated X^- radicals reported herein.

Results and Discussion

Reaction Products Studies. The reactions of $[(CH_3)_3AlX]^-$ (for X = H, CH_3, NH_2, OH, F, SiH_3, PH_2, SH, Cl, and OCH_3) with a variety of acids (HA) are summarized in Table I for the major reaction products. Four different anionic products are observed: (1) A^-, (2) $[(CH_3)_3AlA]^-$, (3) $[(CH_3)_2AlX(A)]^-$, and (4) adducts. Although A^- is observed for every aluminate studied (at least, with some HA), the appearance of X and CH_3 cleavage products depends strongly on X. For X = H, NH_2, OH, PH_2, and OCH_3 there is either exclusive or substantial X cleavage giving $[(CH_3)_3AlA]^-$ in addition to A^- formation. Thus, $[(CH_3)_3AlH]^-$, $[(CH_3)_3AlNH_2]^-$, and $[(CH_3)_3AlPH_2]^-$ give only X cleavage products while $[(CH_3)_3AlOH]^-$ and $[(CH_3)_3AlOCH_3]^-$ give both X and methyl cleavage. For X = F, SiH_3, SH, and Cl, we detect $[(CH_3)_2AlX(A)]^-$ products which are clear indicators of methyl cleavage.

These products can be considered with reference to eqs 2-5 and reaction Scheme II below. Reactions 2 and 3 are potential sources of the A^- products while reactions 4 and 5 formulate the

$$[(CH_3)_3AlX]^- + HA \rightarrow (CH_3)_3Al + A^- + HX \quad (2)$$

$$[(CH_3)_3AlX]^- + HA \rightarrow (CH_3)_2AlX + A^- + CH_4 \quad (3)$$

$$[(CH_3)_3AlX]^- + HA \rightarrow [(CH_3)_3AlA]^- + HX \quad (4)$$

$$[(CH_3)_3AlX]^- + HA \rightarrow [(CH_3)_2AlX(A)]^- + CH_4 \quad (5)$$

formation of the new aluminate products. The adducts listed in Table I are primary products whose structures are unknown. They have m/z = $[(CH_3)_3AlX]^-$ plus HA and are probably ion-dipole and/or hydrogen bonded complexes rather than covalently bound structures.

We have formulated a tentative mechanistic picture to allow us to rationalize the reaction products in terms of eqs 2-5. In this picture (Scheme II), ion-dipole attraction[28] between $[(CH_3)_3AlX]^-$ and HA leads to an adduct in which HA has considerable motion. Such motion allows the acidic H of HA to interact competitively at the X (through I) or the CH_3 (through II) of $[(CH_3)_3AlX]^-$. Protonation on X leads to X cleavage, HX loss, and the formation of a complex of $(CH_3)_3Al$ and A^- (III). The partners in this complex can either dissociate (eq 2) or combine (eq 4). Similarly, protonation on CH_3 leads to methyl cleavage, methane loss, and the formation of a complex of $(CH_3)_2AlX$ and A^- (IV). This complex can either dissociate (eq 3) or associate (eq 5).

We have carried out a limited number of reactions with deuterium-labeled HA's to examine the possibility that various exchange reactions might be occurring without detection (Table I). $[(CH_3)_3AlNH_2]^-$ undergoes exchange with CF_3CD_2OD ($\Delta H°_{acid} \approx$ 362 kcal/mol), CH_3CH_2OD ($\Delta H°_{acid}$ = 377 kcal/mol), and CD_3OD ($\Delta H°_{acid}$ = 384 kcal/mol) leading to $[(CH_3)_3AlNHD]^-$ and $[(CH_3)_3AlND_2]^-$. Exchange also occurs between $[(CH_3)_3AlOH]^-$ and CH_3CO_2D, but not with D_2O. Observation of such reactions indicates that collision complexes like I of $[(CH_3)_3AlNH_2]^-$ and HA are long-lived and form reversibly.[29] Perhaps surprisingly, $[(CH_3)_3AlPH_2]^-$ undergoes only barely detectable exchange with CH_3CO_2D and none with CF_3CO_2D or D_2O.

Computational Aspects of the Thermochemistry. The complexity of these reactions demonstrates that a simple determination of X^- affinities of $(CH_3)_3Al$ based on an analysis similar to that

(24) Krishnan, R.; Binkley, J. S.; Seeger, R.; Pople, J. A. *J. Chem. Phys.* **1980**, *72*, 650-654.
(25) McLean, A. D.; Chandler, G. S. *J. Chem. Phys.* **1980**, *72*, 5639-5648.
(26) Since the TZ basis contains functions nearly as diffuse as those given by Clark et al., we have instead used the still more diffuse exponents given in the following: Dunning, T. H.; Hay, P. J. In *Methods of Electronic Structure Theory*; Schaefer, H. F., Ed.; Plenum Press: New York, 1977; pp 1-27. The polarization functions for C-F were also taken from this reference and these were split by factors of 0.7 and 1.4 to produce 2d sets.
(27) Stewart, J. J. P. *J. Comput. Aided Mol. Design* **1990**, *4*, 1-105.
(28) Su, T.; Bowers, M. T. *Int. J. Mass Spectrom.* **1973**, *12*, 347.
(29) DePuy, C. H.; Bierbaum, V. M. In *Structure/Reactivity and Thermochemistry of Ions*; Ausloos, P., Lias, S. G., Eds.; Reidel Publishing: Dordrecht, Holland, 1987; pp 292-303.

Table I. Reactions of Aluminates with HA

X	HA ($\Delta H°_{acid}$ of HA)	products (branching ratio in %)[a]	cleavage
H	CF_3COOH (323)	CF_3COO^- $[(CH_3)_3AlOC(O)CF_3]^-$	H_2
	CHF_2COOH (331)	CHF_2COO^- $[(CH_3)_3AlOC(O)CHF_2]^-$	H_2
	HCl (333)	Cl^- (7) $[(CH_3)_3AlCl]^-$ (93)	H_2
	HCOOH (345)	$HCOO^-$ (very small) $[(CH_3)_3AlOCHO]^-$	H_2
	$(CH_3)_3CSH$ (352)	no reaction	
	CF_3CH_2OH (362)	adduct	
CH_3	CF_3COOH (323)	CF_3COO^- (41) $[(CH_3)_3AlOC(O)CF_3]^-$ (59)	CH_4
	CHF_2COOH (331)	CHF_2COO^- $[(CH_3)_3AlOC(O)CHF_2]^-$	CH_4
	HCl (333)	Cl^- (31) $[(CH_3)_3AlCl]^-$ (69)	CH_4
	HCOOH (345)	$[(CH_3)_3AlOCHO]^-$	CH_4
	CH_3COOH (348)	$[(CH_3)_3AlOC(O)CH_3]^-$	CH_4
	$(CH_3)_3CSH$ (352)	$[(CH_3)_3AlSC(CH_3)_3]^-$ (very small)	CH_4
	CF_3CH_2OH (362)	$[(CH_3)_3AlOCH_2CF_3]^-$ (small)	CH_4
	CF_3CD_2OD	no reaction	
	CD_3OD (384)	no reaction	
NH_2	HI (314)	I^- $[(CH_3)_3AlI]^-$	NH_3
	CF_3COOH (323)	CF_3COO^- (82) $[(CH_3)_3AlOC(O)CF_3]^-$ (18)	NH_3
	CHF_2COOH (331)	CHF_2COO^- $[(CH_3)_3AlOC(O)CHF_2]^-$ adduct	NH_3
	HCl (333)	Cl^- (27) $[(CH_3)_3AlCl]^-$ (73)	NH_3
	HCOOH (345)	$[(CH_3)_3AlOCHO]^-$	NH_3
	CH_3COOH (348)	$[(CH_3)_3AlOC(O)CH_3]^-$	NH_3
	$CF_3C(O)CH_3$ (349)	$[(CH_3)_3AlCH_2C(O)CF_3]^-$ adduct	NH_3
	H_2S (351)	$[(CH_3)_3AlSH]^-$ (9) adduct (91)	NH_3
	$(CH_3)_3CSH$ (352)	adduct	
	CH_3SH (357)	no reaction	
	CF_3CH_2OH (362)	$[(CH_3)_3AlOCH_2CF_3]^-$ (20) adduct (80)	NH_3
	CF_3CD_2OD	$[(CH_3)_3AlOCH_2CF_3]^-$ adduct $[(CH_3)_3AlNHD]^-$ $[(CH_3)_3AlND_2]^-$	NH_2D
	CHF_2CH_2OH (370)	adduct	
	CH_3CH_2OD (377)	$[(CH_3)_3AlOCH_2CF_3]$ (small) adduct (very small) $[(CH_3)_3AlNHD]^-$ $[(CH_3)_3AlND_2]^-$	NH_2D
	CD_3OD (384)	$[(CH_3)_3AlOCD_3]^-$ (small) adduct (very small) $[(CH_3)_3AlNHD]^-$ $[(CH_3)_3AlND_2]^-$	NH_2D
HO	CF_3COOH (323)	CF_3COO^- $[(CH_3)_3AlOC(O)CF_3]^-$ $[(CH_3)_2Al(OH)OC(O)CF_3]^-$ (small)	H_2O and CH_4
	HNO_3 (325)	NO_3^- $[(CH_3)_3AlNO_3]^-$ $[(CH_3)_2Al(OH)NO_3]^-$ (small) adduct	H_2O and CH_4
HO	CHF_2COOH (331)	CHF_2COO^- $[(CH_3)_3AlOC(O)CHF_2]^-$ $[(CH_3)_2Al(OH)OC(O)CHF_2]^-$ (small) adduct	H_2O and CH_4
	HCl (333)	Cl^- (27) $[(CH_3)_3AlCl]^-$ (33) $[(CH_3)_2Al(OH)Cl]^-$ (20) adduct (20)	H_2O and CH_4
	HCOOH (345)	adduct	
	CH_3COOH (348)	adduct	
	CH_3CO_2D	$[(CH_3)_3AlOD]^-$ (small) adduct	
	D_2O (392)	adduct	
F	CF_3COOH (323)	CF_3COO^- (38) $[(CH_3)_2Al(F)OC(O)CF_3]^-$ (62)	CH_4
	HNO_3 (325)	NO_3^- (39) $[(CH_3)_2Al(F)NO_3]^-$ (61)	CH_4
	CHF_2COOH (331)	CHF_2COO^- (52) $[(CH_3)_2Al(F)OC(O)CHF_2]^-$ (38) adduct (10)	CH_4
	HCl (333)	Cl^- (39) $[(CH_3)_2Al(F)Cl]^-$ (61)	CH_4
	HCOOH (345)	adduct	
	CH_3COOH (348)	adduct	
SiH_3	CF_3COOH (323)	CF_3COO^- $[(CH_3)_2Al(SiH_3)OC(O)CF_3]^-$	CH_4
	HNO_3 (325)	NO_3^- $[(CH_3)_2Al(SiH_3)NO_3]^-$	CH_4
	CHF_2COOH (331)	CHF_2COO^- $[(CH_3)_2Al(SiH_3)OC(O)CHF_2]^-$	CH_4
	HCl (333)	Cl^- (82) $[(CH_3)_2Al(SiH_3)Cl]^-$ (18)	CH_4
	HCOOH (345)	no reaction	
	CH_3CO_2H (348)	no reaction	
PH_2	HI (314)	I^- $[(CH_3)_3AlI]^-$	PH_3
	CF_3COOH (323)	CF_3COO^- $[(CH_3)_3AlOC(O)CF_3]^-$	PH_3
	CF_3COOD (≈323)	CF_3COO^- $[(CH_3)_3AlOC(O)CF_3]^-$ no H/D exchange	PH_2D
	HNO_3 (325)	NO_3^- (very small) $(CH_3)_3AlNO_3^-$	PH_3
	CHF_2COOH (331)	$[(CH_3)_3AlOC(O)CHF_2]^-$	PH_3
	HCl (333)	$[(CH_3)_3AlCl]^-$	PH_3
	HCOOH (345)	$[(CH_3)_3AlOCHO]^-$	PH_3
	CH_3CO_2D	$[(CH_3)_3AlOC(O)CH_3]^-$ (very small) $[(CH_3)_3AlPHD]^-$ (very small)	PH_2D
	CF_3CH_2OH (362)	no reaction	
SH	CF_3COOH (323)	CF_3COO^- (29) $[(CH_3)_2Al(SH)OC(O)CF_3]^-$ (71)	CH_4
	HNO_3 (325)	NO_3^- $[(CH_3)_2Al(SH)NO_3]^-$	CH_4
	CHF_2COOH (331)	$[(CH_3)_2Al(SH)OC(O)CHF_2]^-$ adduct	CH_4
	HCl (333)	Cl^- (22) $[(CH_3)_2Al(SH)Cl]^-$ (78)	CH_4
	HCOOH (345)	adduct	
	CH_3COOH (348)	$[(CH_3)_2Al(SH)OC(O)CH_3]^-$ (very small) adduct (very small)	CH_4
	CH_3COOD	adduct	

Table I. (Continued)

X	HA ($\Delta H°_{acid}$ of HA)	products (branching ratio in %)[a]	cleavage
SH	$(CH_3)_3CSH$ (352)	$[(CH_3)_2Al(SH)SC(CH_3)_3]^-$ (very small)	CH_4
	CF_3CH_2OH (362)	no reaction	
Cl	HI (314)	I^-	CH_4
		$[(CH_3)_2Al(Cl)I]^-$	
	CF_3COOH (323)	CF_3COO^-	CH_4
		$[(CH_3)_2Al(Cl)OC(O)CF_3]^-$	
	CHF_2COOH (331)	CHF_2COO^-	CH_4
		$[(CH_3)_2Al(Cl)OC(O)CHF_2]^-$	
	HCl (333)	Cl^- (7)	CH_4
		$[(CH_3)_2AlCl_2]^-$ (93)	
	HCOOH (345)	adduct	
	CH_3COOH (348)	no reaction	
OCH_3	HI (314)	I^-	CH_3OH
		$[(CH_3)_3AlI]^-$	
	CF_3COOH (323)	CF_3COO^- (16)	CH_3OH and CH_4
		$[(CH_3)_2Al(Cl)OC(O)CHF_2]^-$ (60)	
		$[(CH_3)_2Al(OCH_3)OC(O)CF_3]^-$ (11)	
		adduct (13)	
	HNO_3 (325)	NO_3^-	CH_3OH and CH_4
		$[(CH_3)_3AlNO_3]^-$	
		$[(CH_3)_2Al(OCH_3)NO_3]^-$ adduct	
	CHF_2COOH (331)	$[(CH_3)_3AlOC(O)CHF_2]^-$	CH_3OH and CH_4
		$[(CH_3)_2Al(OCH_3)OC(O)CHF_2]^-$ adduct	
	HCl (333)	$[(CH_3)_3AlCl]^-$ (20)	CH_3OH and CH_4
		$[(CH_3)_2Al(OCH_3)Cl]^-$ (8)	
		adduct (72)	
	HCOOH (345)	$[(CH_3)_3AlOCHO]^-$ (very small)	CH_3OH and CH_4
		$[(CH_3)_2Al(OCH_3)OCHO]^-$ (very small)	
		adduct	
	CH_3COOH (348)	$[(CH_3)_3AlOC(O)CH_3]^-$ (small)	CH_3OH
		adduct	
	CD_3OD (384)	no reaction	

[a] See Experimental Section for details of the branching determinations and their associated errors.

used in Squires' siliconate studies is impossible even though a determination of a series of its X^- affinities would be very informative. To gain a more complete understanding of this reaction chemistry requires a basic understanding of the thermochemistry of aluminates and other aluminum-containing species. We have thus undertaken a number of *ab initio* and semiempirical affinity computations of trivalent aluminum compounds to obtain this information. In addition, *ab initio* computations which can serve as the basis for a thermochemical analysis of eqs 2–5 have been carried out. The computational approach parallels one we used earlier in studies of siliconates.[3] In that study, we computed the X^- affinities (eq 6) of thirteen

$$[H_3SiXY]^- \rightarrow H_3SiY + X^- \quad (6)$$

H_3SiY compounds for thirteen different X groups. Of a total of 91 unique combinations, only five unstable siliconates (X = SiH_3 for Y = OH, CH_3, NH_2, OCH_3, and F) were found using both *ab initio* and MNDO methods. In general, there was a reasonable qualitative correspondence between the *ab initio* results [SCF/6-31G(d) geometries and single point MP2/6-31++G(d,p) energies] and those obtained by MNDO methods. We concluded that the MNDO method gave sufficiently good results to capture substituent trends and to predict the stability of siliconates with respect to their loss of X^- (eq 6). More subtle features of their energetics were successfully gauged only by *ab initio* methods, however.

Ab initio computations at the MP2/6-31++G(d,p) level of the X^- affinities of trimethylaluminum and the Cl^- and CH_3^- affinities of $(CH_3)_2AlX$ are given in Table II (reported at 298 K). The geometries of various aluminates are presented in Table III. The *ab initio* affinity results show certain similarities with the earlier siliconate computational studies even though important differences are revealed as well.[3] Both silane (SiH_4) and trimethylaluminum have larger X^- affinities for the second-row elements than for third-row elements with X = H in an intermediate position. The anion affinities for silicon, however, are generally much smaller than those for aluminum, reflecting both the more electropositive character of aluminum and its electron deficiency in $(CH_3)_3Al$. For example, at the same level of theory, the H^-, CH_3^-, and F^- affinities of CH_3SiH_3 are predicted to be 18, 32, and 29 kcal/mol while trimethylaluminum has corresponding values of 70, 80, and 82 kcal/mol. The series $(CH_3)_2AlX$ has large CH_3^- and Cl^- affinities for all of the X groups studied with the CH_3^- affinity being about 30 kcal/mol larger for all X substituents. In contrast to trimethylaluminum in which the second-row elements have larger X^- affinity values than those of the third-row elements, both $(CH_3)_2AlX$ and H_3SiX have CH_3^- and Cl^- affinities in which the third-row elements have slightly larger affinities than those of the second row.

Table II. Ab Initio MP2 Computations[a] of Anion Affinities for $(CH_3)_2AlX$ and $(CH_3)_3Al$ at 298 K

$[(CH_3)_3AlX]^- \rightarrow (CH_3)_3Al + X^-$ X^- affinity

$[(CH_3)_2Al(Cl)X]^- \rightarrow (CH_3)_2AlX + Cl^-$ Cl^- affinity

$[(CH_3)_3AlX]^- \rightarrow (CH_3)_2AlX + CH_3^-$ CH_3^- affinity

X^-	X^- affinity of $(CH_3)_3Al$ (kcal/mol)	Cl^- affinity of $(CH_3)_2AlX$ (kcal/mol)	CH_3^- affinity of $(CH_3)_2AlX$ (kcal/mol)
H	70	50	81
CH_3	80	50	80
NH_2	84	43	73
OH	84	49	79
F	82	55	86
SiH_3	50	58	91
PH_2	53	56	89
SH	53	54	88
Cl	50	59	93

[a] See Experimental Section for details of the computations.

A few independent experimental measurements support the computational affinity results. The fluoride affinities of AlF_3, BF_3, $(CH_3)_3B$, and $(CH_3CH_2)_3B$ are 117, 79, 47, and 51 kcal/mol, demonstrating that aluminum compounds are stronger Lewis acids than corresponding boron compounds and that alkyl-substituted boranes have smaller fluoride affinities than BF_3.[1] While limited in number, these experimental affinities allow us to estimate a fluoride affinity for $(CH_3)_3Al$ of approximtely 85 kcal/mol, that is about 38 kcal/mol greater than that of $(CH_3)_3B$. This estimate is in good agreement with the computational value of 82 kcal/mol given in Table II. The recent measurement of the hydride affinity of $(CH_3)_3Al$ by Nibbering and co-workers[30] giving a lower limit value of ~85 kcal/mol is difficult to reconcile with the 70 kcal/mol result reported in Table II.

We have also computed the X^- affinities of trimethylaluminum and the CH_3^- affinities of $(CH_3)_2AlX$ using three different

(30) Van Den Berg, K. J.; Ingemann, S.; Nibbering, N. M. M. *Org. Mass Spectrom.* **1992**, *27*, 523–524.

Table III. Ab Initio RHF Aluminum–X Bond Lengths[a] for $(CH_3)_2AlX$ and $[(CH_3)_3AlX]^-$

X	Al–X bond length for $(CH_3)_2AlX$ (Å)	Al–X bond length for $[(CH_3)_3AlX]^-$ (Å)
H	1.59	1.67
CH_3	1.98	2.05
NH_2	1.78	1.89
OH	1.71	1.79
F	1.65	1.71
SiH_3	2.49	2.58
PH_2	2.36	2.48
SH	2.21	2.37
Cl	2.13	2.29

[a] See Experimental Section for details of the computations.

semiempirical methods (MNDO, AM1, and PM3) for X = H, CH_3, NH_2, OH, F, SiH_3, PH_2, SH, and Cl.[27] When these data are compared with the *ab initio* results, we observe essentially no correspondence between computational methods. Although the semiempirical methods capture some of the trends of the *ab initio* computations, they have limited value since they (1) do not give absolute values of affinities which are at all similar to the *ab initio* values, (2) occasionally do not give positive values for certain affinities, and (3) altogether miss many of the trends evident in the *ab initio* data. Furthermore, these methods give results very far out of line for X = NH_2, SiH_3, and Cl, suggesting serious parametrization problems for these substituents in aluminum systems.

Table III presents the Al–X lengths in the tetracoordinate aluminates, $[(CH_3)_3AlX]^-$, as well as in their trivalent counterparts, $(CH_3)_2AlX$. The Al–X bonds and the Al–CH_3 bonds lengthen by 0.06–0.16 Å in going from trivalent to tetravelent aluminum. The Al–X bonds of both $[(CH_3)_3AlX]^-$ and $(CH_3)_2AlX$ shorten as the electronegativity of X increases for the second- and third-row X groups. Each aluminate has nearly tetrahedral geometry about aluminum with methyl groups oriented in the most staggered arrangement possible. The $(CH_3)_2AlX$ species usually arrange the geometry at X so that a lone pair on X (if any) can backbond to the formally vacant p orbital on aluminum. However, the energy penalty to make PH_2 planar is large enough to prevent this sort of partial π bonding in that case.

We have used *ab initio* methods to compute both ΔH_{rxn} and ΔG_{rxn} for the nine aluminates reacting with HCl (eqs 7–9). These

$$[(CH_3)_3AlX]^- + HCl \rightarrow (CH_3)_3Al + Cl^- + HX \quad (7)$$

$$[(CH_3)_3AlX]^- + HCl \rightarrow (CH_3)_2AlX + Cl^- + CH_4 \quad (8)$$

$$[(CH_3)_3AlX]^- + HCl \rightarrow [(CH_3)_3AlCl]^- + HX \quad (9)$$

$$[(CH_3)_3AlX]^- + HCl \rightarrow [(CH_3)_2AlXCl]^- + CH_4 \quad (10)$$

are given in Table IV. The ΔG_{rxn} are reported to provide an estimate of the magnitude of $T\Delta S$ effects. We have chosen to carry out computations on the HCl reactions not only because of their relative computational simplicity but also because each of the aluminates has been studied experimentally with HCl. These reactions are thought to be representative of the wide range of acid cleavages we have studied experimentally.

A comparison of X and CH_3 cleavage in reactions 7 and 8 indicates that the X cleavage is less favorable than the methyl cleavage for all of the X groups studied. Similarly, the X cleavage in reaction 9 leading to a chloroaluminate product is less favored than methyl cleavage in reaction 10 for all X groups. It is likely that the A^- products in these reactions result because the aluminate products of the highly exothermic reaction channels, eqs 9 and 10, cannot always be efficiently stabilized by collisions with helium and thus dissociate. Analysis of reactions 7 and 8 leads to the

Table IV. Ab Initio MP2 Computations[a] of ΔH at 298 K for Reactions 7–10 (ΔG at 298 K Are Given in Parentheses)

X	ΔH_7 (kcal/mol)	ΔH_8 (kcal/mol)	$\delta\Delta H_{8-7}$ (kcal/mol)	ΔH_9 (kcal/mol)	ΔH_{10} (kcal/mol)	$\delta\Delta H_{10-9}$ (kcal/mol)
H	−2.2	−5.2	−3.0	−52	−56	−4
	(−11)	(−14)	(−3)	(−51)	(−56)	(−5)
CH_3	−6.5	−6.5		−56	−56	
	(−17)	(−17)		(−56)	(−56)	
NH_2	12	−14	−26	−38	−57	−19
	(2.6)	(−21)	(−24)	(−37)	(−56)	(−19)
OH	29	−7.4	−37	−21	−57	−36
	(20)	(−16)	(−36)	(−20)	(−56)	(−36)
F	49	−0.1	−49	−0.7	−55	−54
	(39)	(−9.3)	(−48)	(−0.6)	(−55)	(−54)
SiH_3	6.4	4.7	−1.7	−44	−53	−9
	(−3.0)	(−6.5)	(−2.5)	(−42)	(−53)	(−11)
PH_2	16	2.6	−13	−34	−54	−20
	(6.5)	(−6.7)	(−13)	(−33)	(−53)	(−20)
SH	33	1.3	−32	−17	−53	−36
	(23)	(−7.2)	(−30)	(−16)	(−52)	(−38)
Cl	50	6.0	−44	0	−53	−53
	(40)	(−3.2)	(−43)	(0)	(−52)	(−52)

[a] See Experimental Section for details of the computations.

following expressions:

$$\Delta H_7 = \Delta H_{X^-\text{ affinity of }(CH_3)_3Al} + \Delta H^\circ_{acid(HCl)} - \Delta H^\circ_{acid(HX)}$$

$$\Delta H_8 = \Delta H_{CH_3^-\text{ affinity of }(CH_3)_2AlX} + \Delta H^\circ_{acid(HCl)} - \Delta H^\circ_{acid(CH_4)}$$

and suggests that ΔH_8 is always more negative than ΔH_7 mainly because of the very weakly acidic character of methane. For X = NH_2 and OH, where the $\Delta H_{X^-\text{ affinity of }(CH_3)_3Al}$ values (Table II) are greater than the corresponding values of $\Delta H_{CH_3^-\text{ affinity of }(CH_3)_2AlX}$ by 11 and 5 kcal/mol, reaction 7 is less favorable than reaction 8 by 26 and 37 kcal/mol, respectively (compare ΔH_7 and ΔH_8 in Table IV). Here, of course, the difference between $\Delta H^\circ_{acid(HX)}$ and $\Delta H^\circ_{acid(CH_4)}$ also favors reaction 8 over 7 (ΔH°_{acid} of NH_3, H_2O, and CH_4 are 404, 391, and 417 kcal/mol). When X = F, PH_2, SH, and Cl, the situation is different with the $\Delta H_{X^-\text{ affinity of }(CH_3)_3Al}$ values being smaller than the corresponding values of $\Delta H_{CH_3^-\text{ affinity of }(CH_3)_2AlX}$. This situation alone would favor reaction 7 over 8, but the huge ΔH°_{acid} difference between methane and HX more than compensates making reaction 8 favored (ΔH°_{acid} of HF, PH_3, H_2S, and HCl are 371, 371, 351, and 333 kcal/mol). Finally, the cases of X = H and SiH_3 are ones where the affinity and acidity differences are less extreme. For these, the weakly acidic methane term tips the balance in favor of reaction 8, but not by much.

Analogous treatment of reactions 9 and 10 leads to the following expressions:

$$\Delta H_9 = \Delta H_{X^-\text{ affinity of }(CH_3)_3Al} - \Delta H_{Cl^-\text{ affinity of }(CH_3)_3Al} + \Delta H^\circ_{acid(HCl)} - \Delta H^\circ_{acid(HX)}$$

$$\Delta H_{10} = \Delta H_{CH_3^-\text{ affinity of }(CH_3)_2AlX} - \Delta H_{Cl^-\text{ affinity of }(CH_3)_2AlX} + \Delta H^\circ_{acid(HCl)} - \Delta H^\circ_{acid(CH_4)}$$

where again the weakly acidic character of methane plays a dominant role in favoring methane over HX cleavage. The differences between reactions 9 and 10 in Table V vary with X in a way similar to reactions 7 and 8. Since $\delta\Delta H_{8-7}$ records the variation of $(CH_3)_3Al + HX \rightarrow (CH_3)_2AlX + CH_4$ with X and $\Delta\delta H_{10-9}$ records the variation of $[(CH_3)_3AlCl]^- + HX \rightarrow [(CH_3)_2AlXCl]^- + CH_4$ with X, the great similarity in values as X varies is a measure of the internal consistency of our computations.

An interesting relationship is revealed by $\delta\Delta H_{10-9}$, that is, by $[(CH_3)_3AlCl]^- + HX \rightarrow [(CH_3)_2AlXCl]^- + CH_4$. If the heats of this reaction are plotted versus Pauling electronegativities (using the electronegativity of the central atom of each X), we obtain

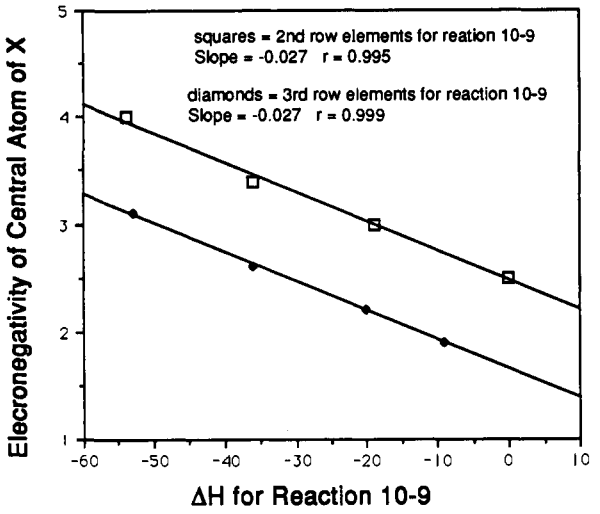

Figure 1. Plot of ΔH_{rxn} for $[(CH_3)_3AlCl]^- + HX \rightarrow [(CH_3)_2AlXCl]^- + CH_4$ versus the Pauling electronegativity of the central atom of X.

two parallel straight lines (Figure 1). One of these corresponds to the X groups of row 2 and the other to those of row 3. Analysis of this reaction gives the following relationship:

$$\Delta H_{10\text{-}9} = \Delta H^\circ_{acid(HX)} - \Delta H_{X^-\text{ affinity of }(CH_3)_2AlCl} - \Delta H^\circ_{acid(CH_4)} + \Delta H_{CH_3^-\text{ affinity of }(CH_3)_2AlCl}$$

Examination of the differences of the first two terms (the only ones varying with X) reveals that these are essentially equal for each periodic group. The difference between $\Delta H^\circ_{acid(HX)}$ and $\Delta H_{X^-\text{ affinity of }(CH_3)_2AlCl}$, the latter calculated from the data in Table IV, is 325 and 315 kcal/mol for CH_3 and SiH_3, 306 and 304 kcal/mol for NH_2 and PH_2, 289 and 289 kcal/mol for OH and SH, and 271 and 272 kcal/mol for F and Cl. Thus, $\Delta H^\circ_{acid(HX)}$ minus $\Delta H_{X^-\text{ affinity of }(CH_3)_2AlCl}$ vary in the same way in a particular periodic group. The relationship seen in Figure 1 is a consequence of the difference in the electronegativities of the second- and third-row elements.

Subtraction of eq 10 from eq 8 gives $[(CH_3)_2AlXCl]^- \rightarrow (CH_3)_2AlX + Cl^-$, which is the Cl^- affinity of $(CH_3)_2AlX$. With values varying from 43 to 59 kcal/mol (Table II), we see that reaction 10 is highly favored over reaction 8 for all X substituents. A similar analysis of reactions 7 and 9 indicates that reaction 9 is favored over 7 by about 50 kcal/mol, the Cl^- affinity of $(CH_3)_3Al$.

Kinetic Studies. Although the methyl cleavage channels are all thermochemically favored over the closely related X cleavage pathways, reaction product studies (Table I) clearly show that cleavage reactions of X occur. Thus, kinetic effects must be considered in any analysis of these reactions. This is not surprising given the complexities of the interactions and structural components of I and II. We have evaluated kinetic effects for a number of these reactions. Of particular interest are the rate coefficients and efficiencies of reaction (an efficiency of 1 means that every collision leads to reaction) for $[(CH_3)_3AlX]^-$ and HCl given in Table V (eqs 7–10). Three of the four third-row aluminates (X = SiH_3, SH, and Cl) have very slow rates, low efficiencies, and give exclusive methyl cleavage. The third-row aluminate with X = PH_2 not only reacts with HCl at least two orders of magnitude faster, but also undergoes X cleavage, suggesting the possibility that all those aluminates undergoing X cleavage might react more rapidly with HCl than those undergoing methyl cleavage. Indeed, all the aluminates that undergo X cleavage have rate coefficients and efficiencies more than two times larger than those undergoing methyl cleavage. For example, $[(CH_3)_3AlF]^-$, $[(CH_3)_3AlSiH_3]^-$, and $[(CH_3)_3AlSH]^-$ have efficiencies of 0.11, 0.002, and 0.004, but the smallest efficiency for X cleavage in Table V is 0.63 for X = PH_2 [or 0.53 if we consider X = OCH_3]. Two aluminates (X = H and NH_2) probably undergo reaction on every collision with HCl. The aluminate $[(CH_3)_4Al]^-$, in which only methyl cleavage can occur, undergoes reaction with HCl with an efficiency of 0.27.

Table V. Rate Coefficients for the Reactions of $[(CH_3)_3AlX]^-$ and HCl

X	$10^9 k_{obs}$[a] (cm^3 molecule^{-1} s^{-1})	k_{obs}/k_{var}[b]	product summary
H	1.2	0.89	X cleavage
CH_3	0.39	0.27	CH_3 cleavage
NH_2	1.2	0.87	X cleavage
OH	0.88	0.62	CH_3 and X cleavage
OD	0.96	0.68	CH_3 and X cleavage
F	0.15	0.11	CH_3 cleavage
SiH_3	0.003	0.002	CH_3 cleavage
PH_2	0.86	0.63	X cleavage
SH	0.006	0.004	CH_3 cleavage
Cl	0.004	0.003	CH_3 cleavage
OCH_3	0.73	0.53	CH_3 and X cleavage

[a] See Experimental section for details of the rate coefficient measurements and their associated errors. [b] Variational computed rate constants are given as k_{var} and calculated according to ref 6.

The rate coefficients and efficiencies of several additional reactions of $[(CH_3)_3AlX]^-$ and HA are given in Table VI. No obvious pattern of reactivity is evident in these data. While the strong acid CF_3CO_2H (ΔH°_{acid} = 323 kcal/mol) reacts with $[(CH_3)_4Al]^-$, $[(CH_3)_3AlNH_2]^-$, and $[(CH_3)_3AlF]^-$ at nearly the collision rate, other strong acids like HNO_3 (ΔH°_{acid} = 325 kcal/mol) and HCl (see above) react much more slowly with some aluminates. Other inconsistent effects are evident with $[(CH_3)_3AlNH_2]^-$ where the weaker acid CF_3CH_2OH (ΔH°_{acid} = 362 kcal/mol) reacts more rapidly than H_2S (ΔH°_{acid} = 351 kcal/mol).

The rate coefficients, efficiencies, and cleavage patterns for the different aluminate reactions present a puzzling reactivity picture. While Scheme II describes some essential features of these reactions, at least in the broadest sense, it does not consider what must be additional subtle features affecting the reaction dynamics. Thus, while four of the five X groups that undergo X cleavage have lone-pair electrons on the atom bonded to aluminum, one, namely X = SH, does not. Inexplicably, the other aluminate that undergoes cleavage has X = H. Among the features that might contribute to these subtleties are the basicity of the X versus the CH_3 groups as well as steric effects and X-to-aluminum delocalization. Since the factors controlling cleavage are not understood, a complete charge density analysis would be particularly useful in pointing out the subtle differences in cleavage reactivity. In the following section, we comment on this in more detail.

Brief Discussion of Electron Densities. Although it is tempting to think that an understanding of the charge distributions in the aluminate anions would allow us to understand their experimental reactivity, unfortunately, it is difficult to define unambiguous atomic charges. For example, Mulliken populations[31] are well-known to be unreliable, particularly in extended basis sets.[32] This scheme assigns charge to the nucleus on which a diffuse function is centered, although this function's spatial distribution may very well extend past its neighboring atoms. In the present case, the Mullikan charges for 6-31G(d), 6-31++G(d,p), and TZ++(2d,p) SCF calculations vary wildly. The charge for Al in $[(CH_3)_3AlF]^-$ is +1.14, +1.26, and +2.28 for these three basis sets. The charge on F in this anion is –0.62, –0.63, and –0.99, whereas the group charge of OH in $[(CH_3)_3AlOH]^-$ is –0.57, –0.48, and –0.94, respectively. It seems unwise to compare these values for any given basis set, since the difference between F and OH for any given basis is also erratic.

(31) (a) Mulliken, R. S. *J. Chem. Phys.* **1955**, *23*, 1833. (b) Mulliken, R. S. *J. Chem. Phys.* **1955**, *23*, 1841.
(32) Reed, A. E.; Weinstock, R. B.; Weinhold, F. *J. Chem. Phys.* **1985**, *83*, 735–746.

Table VI. Rate Coefficients for the Reactions of $[(CH_3)_3AlX]^-$ and HA

X	$10^9 k_{obs}$[a] (cm^3 molecule^{-1} s^{-1}) (HA, $\Delta H°_{acid}$)[b]	k_{obs}/k_{var}[c]	product summary	branching ratio[a,d]
CH_3	1.7 (CF_3CO_2H, 323)	0.89	CH_3 cleavage	$A^-/-CH_3$ = 41/59
NH_2	1.8 (CF_3CO_2H, 323)	0.91	X cleavage	$A^-/-NH_2$ = 82/18
	0.13 (H_2S, 351)	0.08		add/$-NH_2$ = 91/9
	0.56 (CF_3CH_2OH, 362)	0.28		add/$-NH_2$ = 80/20
F	1.7 (CF_3CO_2H, 323)	0.89	CH_3 cleavage	$A^-/-CH_3$ = 38/62
	0.77 (HNO_3, 325)	0.38		$A^-/-CH_3$ = 39/61
	1.7 (CHF_2CO_2H, 331)	0.82		$A^-/-CH_3$/add = 52/38/10

[a] See Experimental Section for details of the rate coefficient and the branching ratio determinations and their associated errors. [b] All the acidities are from ref 5. [c] See Table V and ref 6. [d] $-NH_2$ represent products of the type $[(CH_3)_3AlA]^-$, $-CH_3$ represents products of the type $[(CH_3)_2Al(X)A]^-$, and add represents adducts.

A sounder approach for charge analysis is afforded by the molecular electrostatic potential (MEP).[33] The MEP is the Coulombic force felt by a point positive charge as it approaches another molecule. Since the aluminates are anionic, their MEP extends a long distance. The MEP's outermost contour begins 35 Å from the center of the anion, and at that distance it is spherical. There is nothing to distinguish $[(CH_3)_3AlX]^-$ by its X at long range. At shorter distances, the attractive well at X is somewhat different for X = OH and F. Its depth is −165 and −150 kcal/mol per charge unit, respectively. This small difference exists only at short range, while the long-range contours are nearly identical for these two aluminates. We are, therefore, hesitant to draw conclusions about the preferred reactivity from MEP data.

Reaction Pathway Computational Studies. As a result, we have investigated detailed reaction pathway *ab initio* calculations of reactions 9 and 10 for $[(CH_3)_3AlF]^-$ and $[(CH_3)_3AlOH]^-$ with HCl. These two aluminates were chosen because the experimental results reported herein show OH and methyl cleavage for the former, but only methyl cleavage for $[(CH_3)_3AlF]^-$. Location of the transition states is much more challenging than finding the various minima, and it was felt that these two cases spanned the experimental possibilities. The results of these calculations are shown graphically in Figure 2. All four reactions forming new aluminates are exergonic. Also shown in Figure 2 are the energies of reactions 7 and 8 producing Cl^-. Parts a and b in Figure 2 show the barrier to reaction 9 is 17 kcal/mol while that for reaction 10 is just 6 kcal/mol when X = F. This agrees with the experimental result that no F cleavage is observed for $[(CH_3)_3AlF]^-$. The structures of the transition states for this case are shown in Figure 3 along with the normal mode displacements as the reactants cross each barrier. Both the exiting HF molecule and the newly formed Al–Cl bond are evident in Figure 3a. This is the activated complex corresponding to the unobserved reaction channel 9.

Figure 3b shows a transition state which we assert is for the observed channel 10. The transition frequency for this saddle is much higher than that for reaction 9 and the only motion of the atoms is that for transfer of the hydrogen from HCl to the methyl of $[(CH_3)_3AlF]^-$ which eventually leads to methane formation. The chlorine is located rather far from the aluminum, and it does not possess a large enough normal mode component for this to be seen. Since it is not clear if the chloride will eventually attach to Al (10) or be given off as free Cl^- (8), we carried out intrinsic reaction coordinate (IRC) calculations in the forward direction.[34] The IRC is a steepest descent path in mass-weighted Cartesian coordinate and thus leads from the saddle to products.

We have generated over 100 points on this IRC in an effort to identify what those products are. Selected geometric data along the IRC are summarized in Table VII. During the first 40 points, the transfer of the hydrogen from HCl to give methane is completed (C–H bond of 1.09 Å). However, the methane remains in the vicinity of the aluminum atom, effectively shielding

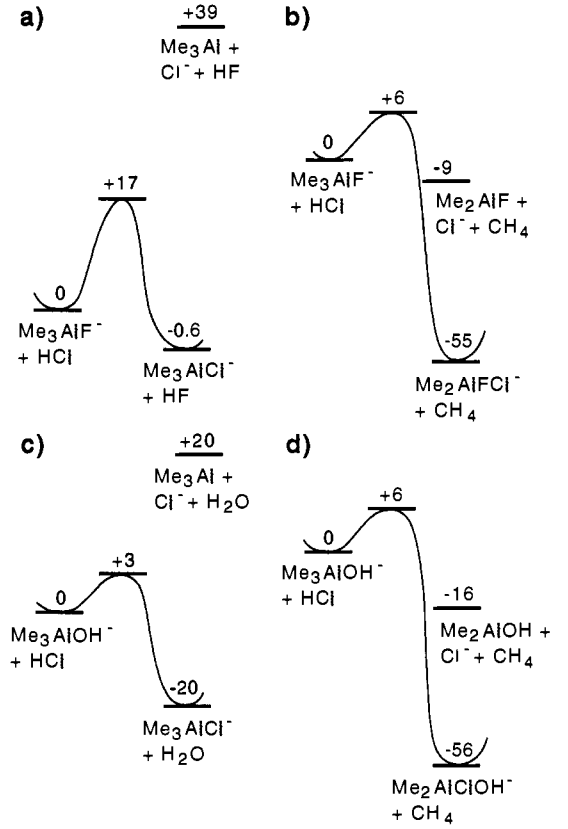

Figure 2. Reaction energy diagrams for $[(CH_3)_3AlF]^-$ and $[(CH_3)_3AlOH]^-$ with HCl (not drawn to scale).

it from chloride attachment. After point 80 on the IRC, the methane slowly begins to move away from aluminum, creating the possibility of chloride attachment. While these changes are occurring, chloride has drifted slightly further away and is now more than 3.5 Å from aluminum. It is not possible, however, that the end point of the IRC is $(CH_3)_2AlF + CH_4 + Cl^-$ since the energy of these three isolated species (−920.381 928) is above the energy at that point on the IRC. Since the system reaches this energy at IRC point 68 and continues to descend, the only plausable endpoint is $[(CH_3)_2Al9F)Cl]^- + CH_4$. Because this particular IRC is excruciatingly slow, we have tested this conclusion by beginning geometry optimizations at the coordinates of IRC points 81 and 105. Both optimizations led to the attachment of the chloride to aluminum once the methane had moved far enough away.

Since the steepest descent path leads to $[(CH_3)_2Al(F)Cl]^- + CH_4$, the transition state shown in Figure 3b is clearly the one leading to the observed products. However, not all reactive trajectories strictly correspond to the steepest descent path. In the present case there must be many trajectories in which slight amounts of extra vibrational energy are transferred to the chloride, causing it to detach somewhere after the transition state is crossed. Such a model accounts not only for the formation of the new aluminate, $[(CH_3)_2Al(F)Cl]^-$, but also for the free Cl^- which is observed experimentally. This appears to be a case where a single

(33) (a) Scrocco, E.; Tomasi, J. *Top. Current Chem.* **1973**, *43*, 95. (b) *Chemical Applications of Atomic and Molecular Electrostatic Potentials*; Politzer, P., Truhlar, D. G., Eds.; Plenum Press: New York, 1981.

(34) Schmidt, M. W.; Gordon, M. S.; Dupuis, M. *J. Am. Chem. Soc.* **1985**, *107*, 2585–2589.

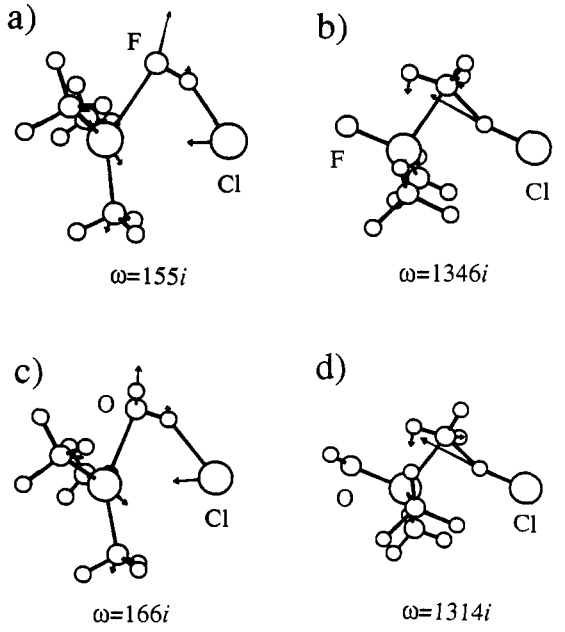

Figure 3. Transition state structures for the reactions of $[(CH_3)_3AlF]^-$ and $[(CH_3)_3AlOH]^-$ with HCl.

Table VII. Intrinsic Reaction Coordinate Computations for the Reaction of $[(CH_3)_3AlF]^-$ and HCl

point	r(Al–C) (Å)	r(C–H) (Å)	r(H–Cl) (Å)	r(Al–Cl) (Å)	energy (hartrees)
transition state	2.19	1.52	1.50	3.56	-920.347 611
6	2.20	1.43	1.60	3.56	-920.349 238
20	2.21	1.27	1.77	3.57	-920.359 669
32	2.22	1.15	1.91	3.57	-920.370 324
46	2.26	1.10	2.03	3.58	-920.376 876
60	2.31	1.10	2.08	3.60	-920.380 266
72	2.35	1.09	2.12	3.62	-920.382 675
90	2.43	1.09	2.19	3.67	-920.387 079
105	2.49	1.09	2.23	3.69	-920.389 461

bottleneck region of the potential surface (Figure 3b) leads to distinct products depending on the exact sequence of events in the exit channel. Both sets of products are exergonic, so there is enough energy in the transition structure in Figure 3b to produce free Cl^-.

For the case of $[(CH_3)_3AlOH]^-$, the barriers to reactions 9 and 10 are the same to within the accuracy of the calculations (±5 kcal/mol). The experimental results indicate that both OH and methyl cleavage occur. The nearly equal barriers for channels 9 and 10 thus agree nicely with the experimental result. The structures in Figure 3c,d are nearly identical to the corresponding X = F transition states. The structures, normal mode components, and transition frequencies are nearly the same, and in fact, X = OH differs from X = F only in the quantitative barrier heights that were shown in Figure 2. Due to the similarity of b and d in Figure 3, we feel that the $[(CH_3)_2Al(OH)Cl]^-$ and free Cl^- observed both arise from the transition structure in Figure 3d.

It is interesting to compare the transition state structures and the IRC analysis with the simple model presented earlier and represented in Scheme II. The transition state model indicates strongly that reactions 7 and 9 have the same transition state as do reactions 8 and 10. Scheme II presented this in a more general way since it was used as a model for all the reactions of HA. Although both models suggest a loose interaction between the aluminate and HA that could lead to reaction at either the methyl or X groups, the IRC result, indicating that methane removal after its formation was slow, was unanticipated in the model summarized by Scheme II. Both models, however, effectively deal with the formation of A^- in these reactions, taking note of the highly exothermic nature of reaction paths 4 and 5 in explaining A^- formation.

Summary. Cleavage reactions of X and/or CH_3 occur when $[(CH_3)_3AlX]^-$ and acids react. Complex cleavage reactivity patterns have been experimentally observed although *ab initio* computational studies clearly show that CH_3 cleavage is favored for widely varying X substituents. *Ab initio* studies of reaction pathways show that a higher barrier to F than CH_3 cleavage occurs in the reaction of $[(CH_3)_3AlF]^-$ and HCl, but that the OH and CH_3 barriers are about the same in the reaction of $[(CH_3)_3AlOH]^-$ and HCl. These results are consistent with the experimental observations that only CH_3 cleavage occurs when X = F, but both OH and CH_3 cleavage occur when X = OH.

Acknowledgment. R.D. thanks the National Science Foundation (CHE-8921522) and the donors of the Petroleum Research Fund, administered by the American Chemical Society, for support of this work. M.S.G. was supported by the Air Force Office of Scientific Research (AFOSR 90-0052). The calculations were performed on the North Dakota State University IBM 3090/200E, obtained in part with the aid of a Joint Study Agreement with IBM (M.S.G. and M.W.S.), as well as on a DEC Station 3100 and an IBM RS 6000/530, obtained by grants to M.S.G. from the Air Force Office of Scientific Research.